crystals

MDPI

Article

Interplay between Structural, Electronic, and Magnetic Properties in the p^0-d Semi-Heusler Compounds: The Case of Li-Based Compounds

Kemal Özdoğan [1,†] and Iosif Galanakis [2,*,†]

[1] Department of Physics, Yildiz Technical University, 34210 İstanbul, Turkey; kozdogan@yildiz.edu.tr
[2] Department of Materials Science, School of Natural Sciences, University of Patras, GR-26504 Patra, Greece
* Correspondence: galanakis@upatras.gr
† These authors contributed equally to this work.

Abstract: Half-metallic semi-Heusler compounds (also known as half-Heusler compounds) are currently at the forefront of scientific research due to their potential applications in spintronic devices. Unlike other semi-Heuslers, the $p^0(d^0)$-d compounds do not appear to crystallize in the typical variant of the $C1_b$ structure. We investigate this phenomenon in the p^0-d Heusler compounds LiYGa and LiYGe, where Y varies between Ca and Zn, using first-principles ab initio electronic band-structure calculations. We examine the electronic and magnetic properties of these compounds in relation to the three possible $C1_b$ structures. Notably, LiVGa, LiVGe, LiMnGa, and LiCrGe are half-metallic ferromagnets across all three variations of the $C1_b$ lattice structure. Our findings will serve as a foundation for future experimental studies on these compounds.

Keywords: Heusler compounds; ab initio calculations; first principles; electronic structure; magnetic materials; Slater–Pauling rule

check for updates

Citation: Özdoğan, K.; Galanakis, I. Interplay between Structural, Electronic, and Magnetic Properties in the p^0-d Semi-Heusler Compounds: The Case of Li-Based Compounds. *Crystals* **2024**, *14*, 693. https://doi.org/10.3390/cryst14080693

Academic Editor: Raphaël P. Hermann

Received: 15 July 2024
Revised: 26 July 2024
Accepted: 28 July 2024
Published: 29 July 2024

Copyright: © 2024 by the authors. Licensee MDPI, Basel, Switzerland. This article is an open access article distributed under the terms and conditions of the Creative Commons Attribution (CC BY) license (https://creativecommons.org/licenses/by/4.0/).

1. Introduction

In the early 20th century, German metallurgist Heusler made a groundbreaking discovery while researching ways to enhance the electrical conductivity of steel [1,2]. He identified a novel compound, Cu_2MnAl. As the century progressed, advancements in instrumentation revealed that Cu_2MnAl possesses a face-centered cubic (f.c.c.) lattice structure, similar to well-known semiconductors like Si and GaAs. This lattice structure is also found in various intermetallic compounds with unique properties, which became known as "Heusler compounds" or "Heusler alloys" [3–5]. Many Heusler compounds notably exhibit ferromagnetic properties with high Curie temperatures. They can be classified into four distinct families based on the number and valence of their constituent atoms:

1. Semi-Heusler (also known as half-Heusler) compounds, such as NiMnSb, follow the XYZ chemical formula. Here, X and Y represent transition metal atoms or lanthanides, while Z is a metalloid. The lattice structure of semi-Heusler compounds is denoted as "$C1_b$".
2. Full-Heusler compounds, such as Co_2MnSi, have the chemical formula X_2YZ, with the X, Y, and Z atoms similar to those in semi-Heuslers. These compounds crystallize in the "$L2_1$" lattice structure.
3. Inverse Heuslers are similar to full-Heuslers, but the valence of X is smaller than that of Y. Their lattice structure is known as "XA" or "$X\alpha$".
4. Ordered equiatomic quaternary Heusler compounds, such as (CoFe)TiSi, are represented by the chemical formula $(XX')YZ$ and crystallize in the "LiMgPdSn" structure [4,6].

In all these Heusler compound families, the metalloid atom Z plays a significant role. Recently, the possibility of replacing the metalloid atom with a transition metal has been explored, leading to the so-called all-d-metal Heusler compounds [7–9].

In the early 21st century, interest in Heusler compounds surged, largely due to the discovery that half-metallicity is a common feature among various ferromagnetic and ferrimagnetic Heusler compounds [10,11]. Half-metallic compounds exhibit metallic behavior for majority spin electrons while displaying semiconducting characteristics for minority spin electrons [12]. This unique property results in a high degree of spin polarization at the Fermi level, making them particularly attractive for spintronics and magnetoelectronics applications by introducing novel functionalities to electronic devices. While other materials have been explored for their half-metallic properties, Heusler compounds offer distinct advantages due to their high Curie temperatures. Consequently, extensive research has focused on investigating their fundamental properties and potential applications [13–16]. Recent studies suggest that certain magnetic Heusler compounds may exhibit even more unconventional behaviors beyond half-metallicity, such as spin-gapless semiconducting and spin-filtering properties, introducing entirely new functionalities with promising implications for various applications [17].

First-principles calculations, also known as ab initio calculations, are a powerful method for understanding material properties and predicting the development of new compounds with tailored characteristics. Recently, numerous extensive databases based on first-principles calculations have emerged, encompassing hundreds of magnetic Heusler compounds [18–24]. These compounds show significant promise in the fields of spintronics and magnetoelectronics. These databases complement studies that primarily focus on understanding the fundamental origins of these compounds' properties, which typically investigate a relatively limited number of Heusler compounds [10,11].

Modern growth techniques have enabled the realization of thin-film compounds, initially conceived through theoretical predictions. For example, (CrV)TiAl, a quaternary Heusler compound, was predicted in Ref. [25] to be a fully-compensated ferrimagnetic semiconductor. It was later successfully synthesized, and its distinctive magnetic properties were confirmed, as detailed in Ref. [26]. This success highlights the strong rationale for exploring novel Heusler compounds that might exhibit unique properties. As previously mentioned, in magnetic Heusler compounds, X typically represents a transition metal or rare earth element. However, within the family of semi-Heusler compounds, X can sometimes be replaced entirely with an alkali or alkaline-earth atom. These particular compounds are referred to as "p^0-d or d^0-d Heusler compounds". The term p^0 refers to elements like Li, Be, Na, and Mg, while d^0 refers to elements such as K, Rb, Cs, Ca, Sr, and Ba, indicating the character of the first empty states in the free atom.

Damewood et al. [27] and Dehghan and Davatolhagh [28] studied compounds like LiMnPt, SrVSb, and KMnP using ab initio electronic structure calculations. In Ref. [29], Dehghan and Davatolhagh created a database containing 420 XYZ d^0-d Heusler compounds, where X was one of K, Rb, or Cs, Y was a transition metal atom, and Z was a group-IV, -V, or -VI element. Among these, 98 were identified as half-metals following the $M_t = Z_t$-8 Slater–Pauling rule ($M_t = Z_t$-18 when Y was Cu or Zn) [30]. In 2022, the same group expanded their database to include p^0-d semi-Heusler compounds, where X was one of Li, Be, Na, or Mg, and Z was a group-V or group-VI element [31]. Although databases are extremely useful due to the large number of compounds studied, they do not analyze in depth the properties of the compounds. Motivated by the above-mentioned results, our present study focuses on the LiYGa and LiYGe compounds, where Y is a 3d transition metal atom ranging from Sc to Zn. For completeness, we also consider the case where Y is Ca, an alkaline-earth element. The rationale behind this focus lies in the remarkable properties exhibited by these compounds, making them well suited for applications in spintronics and magnetoelectronics. Our research comprehensively examines various facets of these compounds, including their structural, electronic, and magnetic properties. We do not include in our study the calculation of the Curie temperature for the magnetic compounds, since this is a tedious task involving the determination of the exchange constants as in Reference [32] and exceeds the scope of the present study.

2. Computational Details

Our research is dedicated to investigating the ground-state properties of Li-based semi-Heusler compounds. To accomplish this, we employ the full-potential nonorthogonal local-orbital minimum-basis band-structure approach (FPLO) for our first-principles electronic band-structure calculations (version FPLO14.00-47), as outlined in Refs. [33,34]. In these calculations, we apply the generalized gradient approximation (GGA) as the exchange-correlation functional within the Perdew–Burke–Ernzerhof (PBE) parameterization [35]. This choice is well known for yielding precise outcomes, especially when dealing with half-metallic Heusler compounds, aligning closely with experimental observations [10,11]. To ensure the accuracy of our calculations, the total energy is converged to the 10th decimal point. Furthermore, a dense grid of **k**-points, specifically a $20 \times 20 \times 20$ grid, according to the Monkhorst–Pack scheme [36], is utilized for the integrals in reciprocal space. Here, we should note that we have only considered the case of ferromagnetic alignment of the spin magnetic moments of the Y elements in both families of LiYGa and LiYGe compounds. This assumption is valid since all known semi-Heusler compounds, where Y is a transition metal atom, present ferromagnetic and not antiferromagnetic order of the Y spin magnetic moments [3,4].

3. Results and Discussion

3.1. Structural Properties

Semi-Heusler compounds, as mentioned above, crystallize in the $C1_b$ lattice structure where one of the four inequivalent sites is vacant. Depending on the sequence of the atoms, there are three variants of the $C1_b$, which are widely known as the α, β, and γ phases. All three phases are presented in Figure 1. Each A and C site (black spheres and black squares in the figure) is at the center of a cube surrounded by four B (pink spheres) and four D (green spheres) sites. Each A(C) site has as second neighbors six C(A) sites. The same reasoning applies to the nearest and next-nearest neighbors of the B and D sites. Thus, in all cases, the tetrahedral symmetry is present, and what alters is the local environment of the atoms and thus the interactions (hybridization) between the orbitals located at the nearest neighbors.

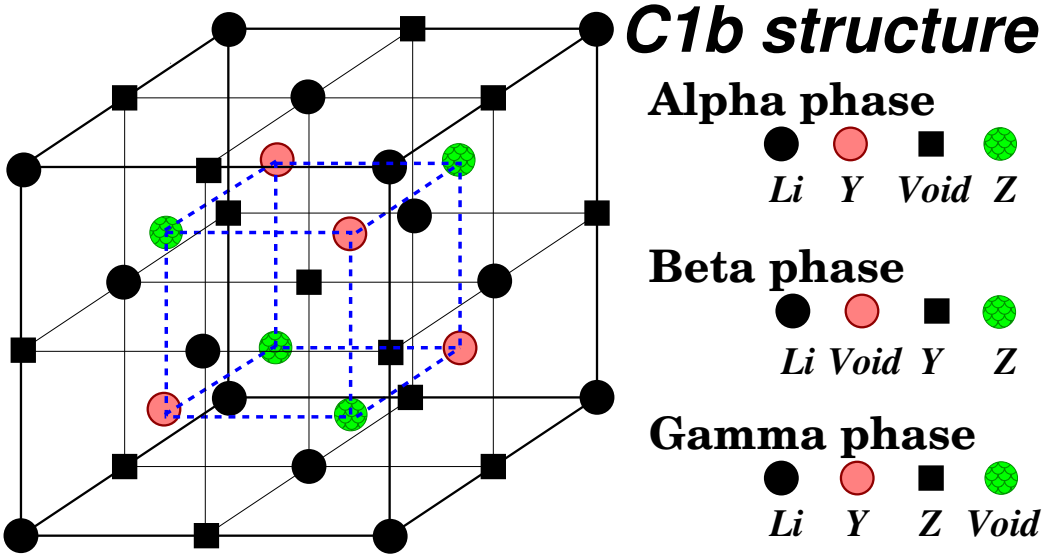


Figure 1. Schematic representation of the three possible phases of the $C1_b$ structure adopted by the semi-Heusler compounds. The black spheres, pink spheres, black squares, and green spheres are widely called A, B, C, and D sites, respectively. The large cube in the figure contains exactly four primitive unit cells.

For all 22 compounds under study and for all three phases, we determined the equilibrium lattice constant using total energy calculations; the former is the lattice constant for

which the total energy is minimum. In Table 1, we present our results. First, we should note that the lattice constants range between 5.42 Å and 7.14 Å and thus are in the same range as most of the well-known Heusler compounds and binary semiconductors, which is useful for practical applications where multilayers are used. The Ga compounds have slightly larger values of the equilibrium lattice constant compared to the corresponding Ge ones. This is expected since Ga has a slightly larger atomic radius as a free atom compared to Ge. If one now keeps Ga or Ge fixed and varies Y between Ca and Zn, the lattice constants follow the trend of the atomic radius of the free atoms. The equilibrium lattice constant decreases as we move from Ca to V and then increases as we move from V to Zn. If now compares the three phases, the only safe conclusion is that the α phase, where Li has four Y and four Ga/Ge atoms as nearest neighbors, also corresponds to the smallest equilibrium lattice constant. If we compare the β and γ phases, there is no clear trend, although in most cases, the β phase corresponds to larger lattice constants. In these two phases, each Li atom has as nearest neighbors four vacant sites (voids in Figure 1) and four Y or four Ga/Ge atoms for the β and γ phases, respectively.

Table 1. We provide the equilibrium lattice constants for all compounds under study in the α, β, and γ phases. The next three columns present the total energy difference between the two phases using the equilibrium lattice constant for each.

Compound	**Lattice Constant a in Å**			**Energy Difference ΔE in eV**			**Most Stable**	**Least Stable**
LiYZ	**α Phase**	**β Phase**	**γ Phase**	$E_\beta - E_\alpha$	$E_\beta - E_\gamma$	$E_\alpha - E_\gamma$	**Phase**	**Phase**
LiCaGa	6.72	7.00	7.14	−0.13	−0.86	−0.73	β	γ
LiScGa	6.13	6.42	6.52	−0.17	−1.04	−0.87	β	γ
LiTiGa	5.80	6.06	6.17	−0.28	−1.00	−0.72	β	γ
LiVGa	5.69	5.93	6.03	−0.30	−0.67	−0.37	β	γ
LiCrGa	5.84	6.08	6.17	−0.35	−0.36	−0.01	β	γ
LiMnGa	5.78	5.95	5.99	−0.31	−0.28	0.03	β	α
LiFeGa	5.66	5.81	5.89	−0.42	−0.06	0.36	β	α
LiCoGa	5.44	5.63	5.66	−0.66	−0.04	0.63	β	α
LiNiGa	5.55	5.69	5.71	−0.55	0.19	0.74	γ	α
LiCuGa	5.75	5.87	5.87	−0.32	0.29	0.61	γ	α
LiZnGa	5.97	6.06	6.05	−0.32	0.09	0.41	γ	α
LiCaGe	6.49	6.86	6.94	−0.08	−1.10	−1.03	β	γ
LiScGe	5.98	6.31	6.38	−0.41	−1.24	−0.83	β	γ
LiTiGe	5.72	6.01	6.10	−0.48	−0.94	−0.46	β	γ
LiVGe	5.69	5.96	5.98	−0.61	−0.76	−0.15	β	γ
LiCrGe	5.72	5.94	5.95	−0.59	−0.51	0.08	β	α
LiMnGe	5.76	5.99	5.96	−0.49	−0.30	0.19	β	α
LiFeGe	5.59	5.75	5.76	−0.62	−0.04	0.58	β	α
LiCoGe	5.42	5.59	5.58	−0.93	0.06	0.98	γ	α
LiNiGe	5.49	5.65	5.62	−0.68	0.25	0.93	γ	α
LiCuGe	5.67	5.81	5.77	−0.47	0.31	0.78	γ	α
LiZnGe	5.88	6.00	5.96	−0.58	0.06	0.64	γ	α

Finally, we should comment on the relative stability of the three possible phases. In Table 1, we include the energy differences in eV units between the three phases expressed per formula unit. A minus sign means that the phase corresponding to the first total energy is the most stable of the two phases compared. The absolute energy differences in all cases are below 1 eV. Although this value may seem quite small, this is not really the case. At room temperature, the thermal energy $k_B T = 0.0259$ eV is much smaller than most of the values in Table 1. Thus, at room temperature, the thermal energy provided to the compound is not enough to overcome the energy barrier and adopt another phase. One may envisage that this could be achieved by growing low-dimensional samples, such as thin films and nanostructures.

To make the behavior of the compounds in the last two columns of Table 1 clearer, we present the most and least stable structures for all compounds under study. We see that for both the LiYGa and LiYGe compounds, there is a clear trend. For most of them, the β phase is the most stable, as is also the case for most of the p^0-d and d^0-d compounds studied in the literature [27–29,31]. For the lighter Y elements, the least stable is the γ phase. As we move to heavier elements, the γ phase first becomes energetically more favorable than the α phase, and for the heaviest atoms, its total energy becomes even lower than the β phase, and it is now the most stable phase.

3.2. Electronic Properties

At the equilibrium lattice constants, we performed electronic band-structure calculations for all twenty-two compounds within our study. Subsequently, we extracted the total density of states (DOS) per formula unit (f.u.), which is visually represented in Figure 2 for the LiYGa compounds and in Figure 3 for the LiYGe compounds. For each compound, we performed calculations for the α, β, and γ phases presented in the three different columns in the two figures. In all cases, there is also some DOS weight around -6 to -9 eV, which corresponds to one s-state per spin direction stemming from the Li atom, which is not shown in the figures.

Overall, the total DOS in the window we show is governed by p-d hybrids created between the p-states of the Ga/Ge atoms and the d-states of the transition-metal atom. In the case of tetrahedral symmetry, the valence d-states split into the double-degenerate e_g and the triple-degenerate t_{2g} states. The latter transform following the same representation as the valence p states of the Ga/Ge atoms, and thus they are allowed to hybridize and create new states that spread across the transition metal and the Ga/Ge atoms. In the case of the LiCaGa and LiCaGe compounds, the Ca atoms have no valence d-states, and the DOS shown in Figures 2 and 3 is due to the interaction p-p of the Ca and Ga/Ge valence p-states. Finally, in the case where Y is Cu, all d-states are occupied and thus are low in energy, and the DOS at the Fermi level is very low. This is even more pronounced in the case of the LiZnGa and LiZnGe compounds, where the Zn valence d-states shift even deeper in energy and are below the energy window shown in the figures.

As can be easily deduced from the DOS in the two figures, most of the compounds are semiconductors (identical DOS for both spin directions), and only a few are magnetic. For magnetism to be favorable, usually the Stoner criterion must be valid, and the DOS at the Fermi level in the magnetic case should result in lower total energy than in the non-magnetic case. We discuss in detail the magnetic properties in the next subsection. Among the magnetic compounds, a few are half-metals or almost half-metals possessing a gap in the spin-down band structure. A detailed analysis of the DOS around the Fermi level reveals that perfect half-metallicity is found in the case of LiCaGe in both the β and γ phases, in the case of LiScGa only in the β phase (in the γ phase, it is close to half-metallicity), and in the case of LiVGa/LiVGe/LiCrGe in all three phases. The LiMnGa and LiMnGe compounds are also close to half-metallicity, except for LiMnGa in the β phase, which is a perfect half-metal since the Fermi level slightly crosses the band just below or just above the spin-down energy gap.

Finally, we should briefly comment on the behavior of the DOS as a function of the three phases. Overall, the DOS between the β and γ phases are similar. The common feature of these two phases is that the Y and Ga/Ge atoms are nearest neighbors. This leads to similar bonding between the valence states of these atoms and thus to similar DOS. The Li atoms contribute only with the s-states very deep in energy. Thus, its different local environment in the two phases plays no crucial role in the shape of the DOS. The shape of the DOS for the α phase, where the Y and Ga/Ge atoms are next-nearest neighbors, has more pronounced differences. Thus, one can conclude that the reason the most stable structure for all twenty-two compounds, as presented in Table 1, is either the β or the γ phase is the stronger bonding between the Y and Ga/Ge atoms, which are now nearest neighbors.

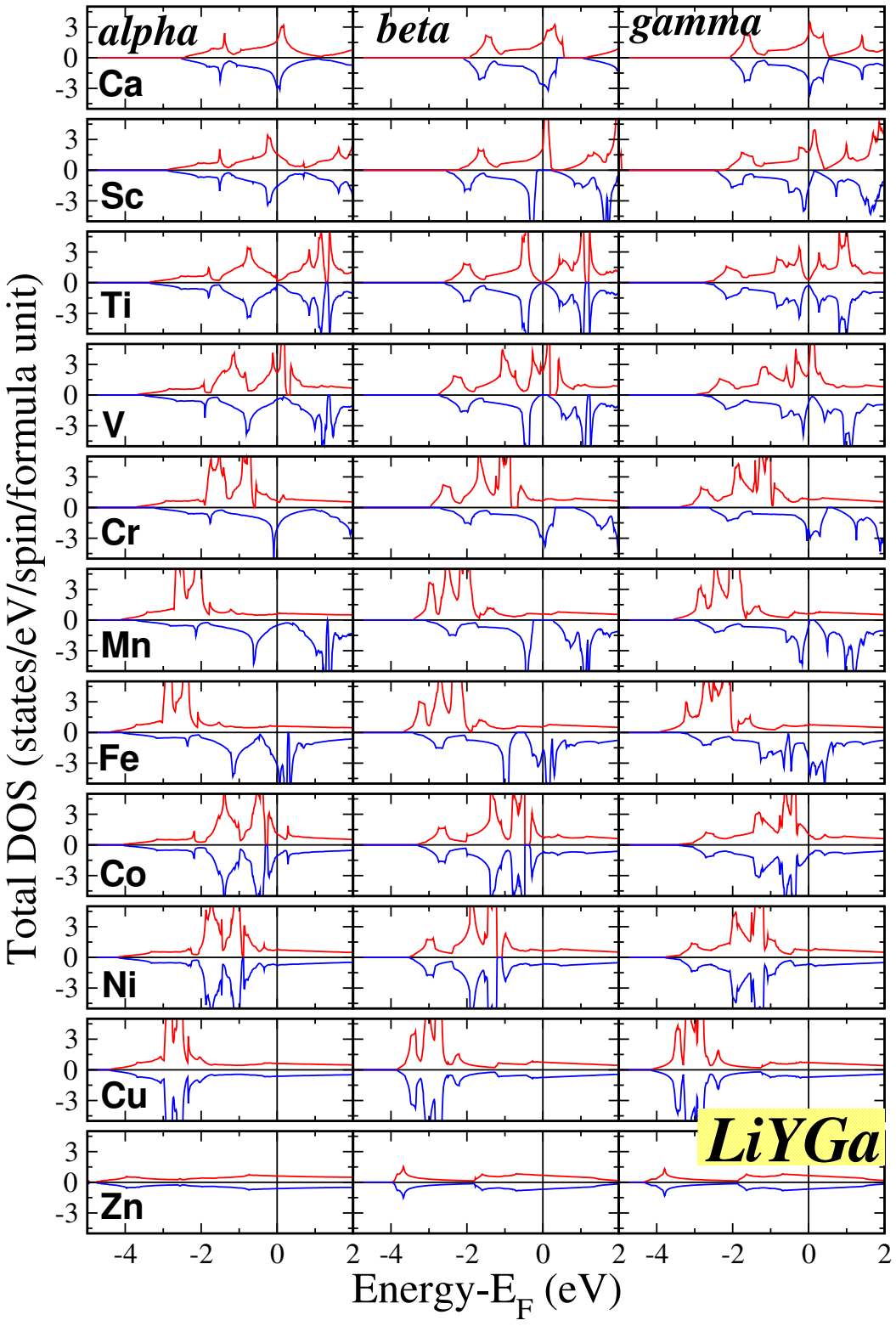


Figure 2. Total density of states (DOS) for the Li*Y*Ga compounds for all three phases. The zero energy has been assigned to the Fermi level. Positive (negative) DOS values correspond to the spin-up (spin-down) electrons.

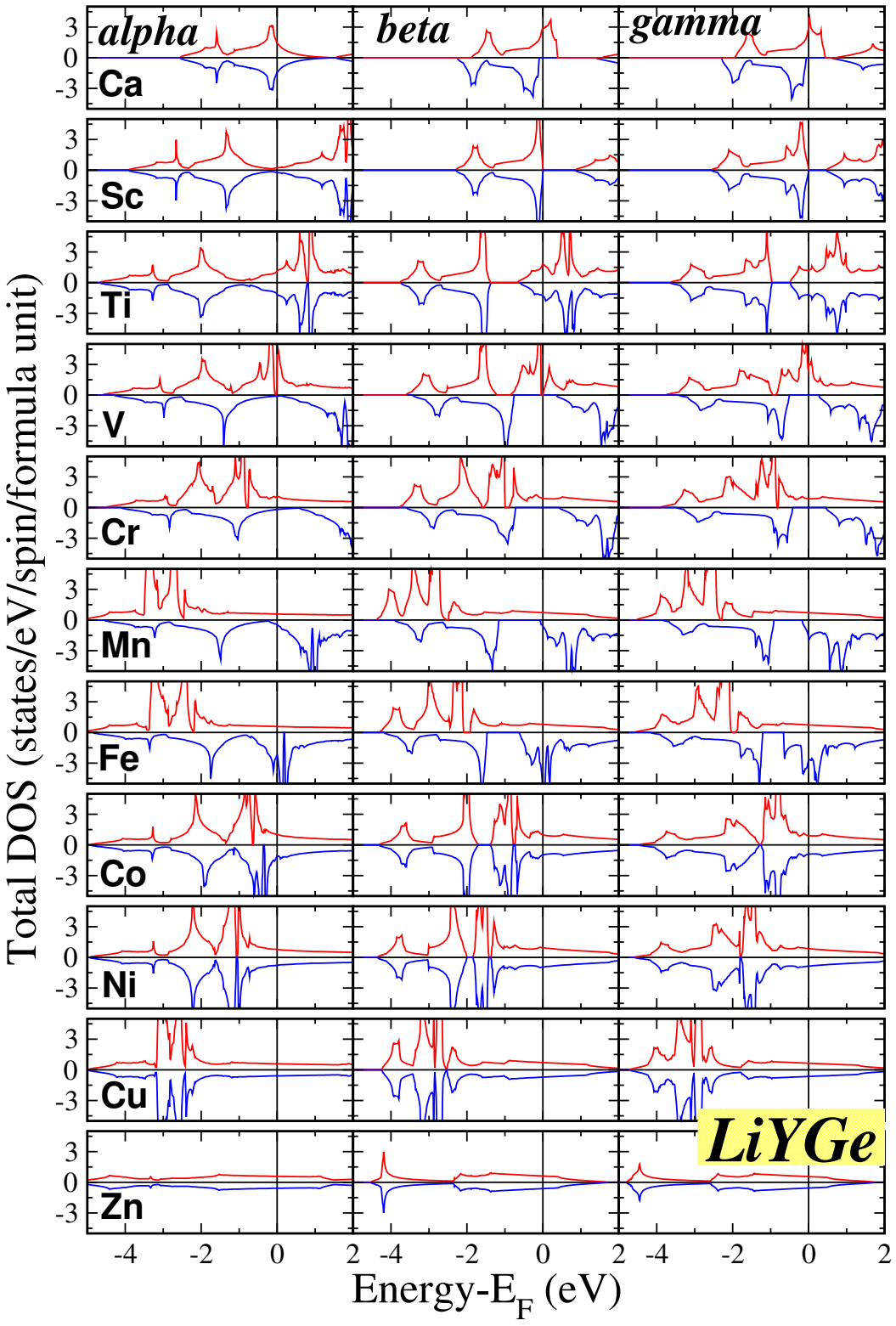


Figure 3. Same as Figure 2 but for the LiYGe compounds.

3.3. Magnetic Properties

As discussed above, most of the compounds are semiconductors. In Table 2, we provide the computed atomic and total spin magnetic moments for all magnetic compounds, employing their equilibrium lattice constants for each phase. In all cases, the Ga/Ge atoms carry a large portion of the total spin magnetic moment, as expected, since the Ga/Ge-p – Y-t_{2g} hybrids have considerable weight also at the Ga/Ge sites. Only in the case of heavier transi-

tion metal atoms like V, Cr, Mn, and Fe is the spin magnetic moment mainly concentrated at the Y atom. As is also the case for most of the Heusler compounds, the Y and Ga/Ge spin magnetic moments are antiparallel when Y is a transition metal atom, with the exception of Sc. The Li atoms also carry small spin magnetic moments that can be safely neglected, with the exception of the LiMnGa and LiFeGa compounds. Here, we should also mention that for LiCaGa, LiCaGe, and LiScGa, the spin magnetic moments shown in Table 2 have negative signs. Although this makes no sense since all are parallel for these three compounds, we adopted this convention in order to be consistent with the Slater–Pauling rule discussed in the next paragraph since these compounds have less than eight valence electrons per formula unit.

Table 2. For the compounds being magnetic we provide the atom-resolved spin magnetic moments in μ_B units, as well as the total spin magnetic moment m^{total} per formula unit, which coincides with the per unit cell value. The last two columns are the total number of valence electrons in the unit cell, Z_t, as well as the ideal total spin magnetic moment if the Slater–Pauling rules were valid, m^{S-P}. The cases not presented in the table have both zero atomic and total spin magnetic moments.

Compound	Phase	m^{Li}	m^{Y}	$m^{Ga/Ge}$	m^{total}	Z_t	m^{S-P}
LiCaGa	α	−0.062	−0.046	−0.134	−0.242	6	−2
	β	−0.068	−0.066	−0.282	−0.417	6	−2
LiCaGe	β	−0.006	−0.091	−0.903	−1.000	7	−1
	γ	0.008	−0.176	−0.832	−1.000	7	−1
LiScGa	β	−0.076	−0.458	−0.466	−1.000	7	−1
	γ	−0.089	−0.388	−0.271	−0.748	7	−1
LiTiGe	β	0.008	0.135	−0.022	0.121	9	1
LiVGa	α	0.006	1.332	−0.237	1.101	9	1
	β	−0.066	1.288	−0.222	1.000	9	1
	γ	−0.001	1.311	−0.232	1.078	9	1
LiVGe	α	0.066	2.404	−0.426	2.044	10	2
	β	0.023	2.438	−0.461	2.000	10	2
	γ	0.104	2.362	−0.466	2.000	10	2
LiCrGa	α	−0.073	3.835	− 0.422	3.340	10	2
	β	−0.190	3.933	−0.348	3.396	10	2
	γ	−0.002	4.203	−0.280	3.921	10	2
LiCrGe	α	−0.013	3.747	−0.596	3.138	11	3
	β	−0.030	3.697	−0.667	3.000	11	3
	γ	0.076	3.636	−0.712	3.000	11	3
LiMnGa	α	−0.204	3.979	−0.511	3.264	11	3
	β	−0.227	3.830	−0.603	3.000	11	3
	γ	−0.125	3.768	−0.625	3.018	11	3
LiMnGe	α	−0.028	4.264	−0.343	3.892	12	4
	β	−0.034	4.290	−0.317	3.940	12	4
	γ	0.089	4.054	−0.427	3.717	12	4
LiFeGa	α	−0.160	2.986	−0.254	2.572	12	4
	β	−0.154	2.748	−0.333	2.261	12	4
	γ	−0.093	2.785	−0.287	2.406	12	4
LiFeGe	α	−0.088	2.978	−0.189	2.701	13	5
	β	−0.055	2.640	−0.244	2.342	13	5
	γ	0.024	2.604	−0.254	2.326	13	5
LiCoGe	α	−0.018	0.395	−0.053	0.324	14	7

Following the discussion of the total spin magnetic moments per formula unit in Refs. [10,30], we now focus on the behavior of the total spin magnetic moment M_t per formula unit. To make our discussion clearer, in Table 2, we provide the total number of valence electrons per unit cell (which coincides with the per formula unit value), Z_t,

and the total spin magnetic moment expected by the Slater–Pauling rule. In Figure 4, we plot the total spin magnetic values for all compounds under study as a function of the *Y* element and compare them with the values expected from the Slater–Pauling rules. For the magnetic compounds (total spin magnetic moment does not vanish), when the calculated and the Slater–Pauling rule-derived total spin magnetic moment values coincide, one would expect that perfect half-metallicity is present. This is true if we compare the total spin magnetic moments with the DOS presented in the previous subsection. Interestingly, as can be deduced from Figure 4, there are four compounds—LiVGa, LiMnGa, LiVGe, and LiCrGe—that have either integer values of their total spin magnetic moments or almost integer values in all three phases and thus are either perfect half-metals or almost perfect half-metals. These compounds are of particular interest since they could find applications in spintronic and magnetoelectronic devices since half-metallicity is independent of the grown phase.

To elucidate the origin of the spin-down gap in the half-metallic compounds and thus the origin of the Slater–Pauling rule, we should perform an analysis similar to the one for other half-metallic Heusler compounds [30]. When *Y* is Ca to Ni, in the spin-down electronic band structure, there are exactly four fully occupied states. The first one stems from the *s* valence state of Li, and the following three stem from the p-t_{2g} hybridization between the Ga/Ge and the *Y* atoms (p-p in the case where *Y* is Ca). Thus, the number of non-compensated spins that coincide with the total spin magnetic moment per unit cell is $M_t = Z_t - 2 \times 4 = Z_t - 8$. When *Y* is Cu or Zn, for perfect half-metallicity to occur, all *d* valence states should be occupied, and the Slater–Pauling rule now becomes $M_t = Z_t - 2 \times 9 = Z_t - 18$. Of course, as discussed above when *Y* is Co, Ni, Cr, or Zn, the DOS at the Fermi level for the non-magnetic case is quite low, and thus no tendency to magnetism is present.

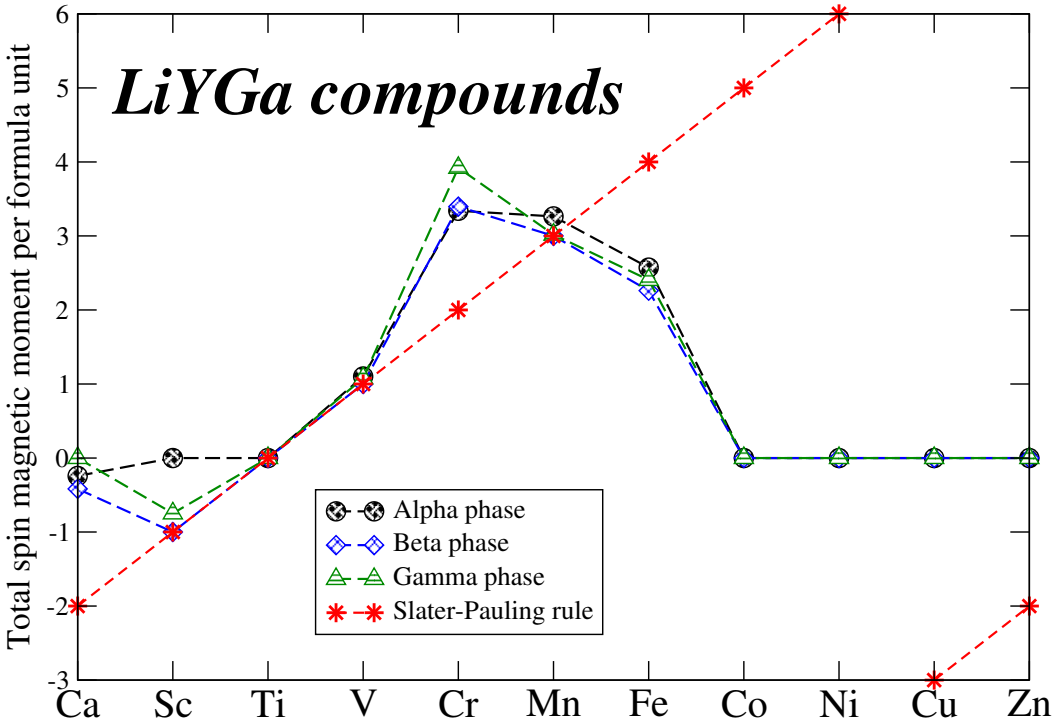


Figure 4. *Cont.*

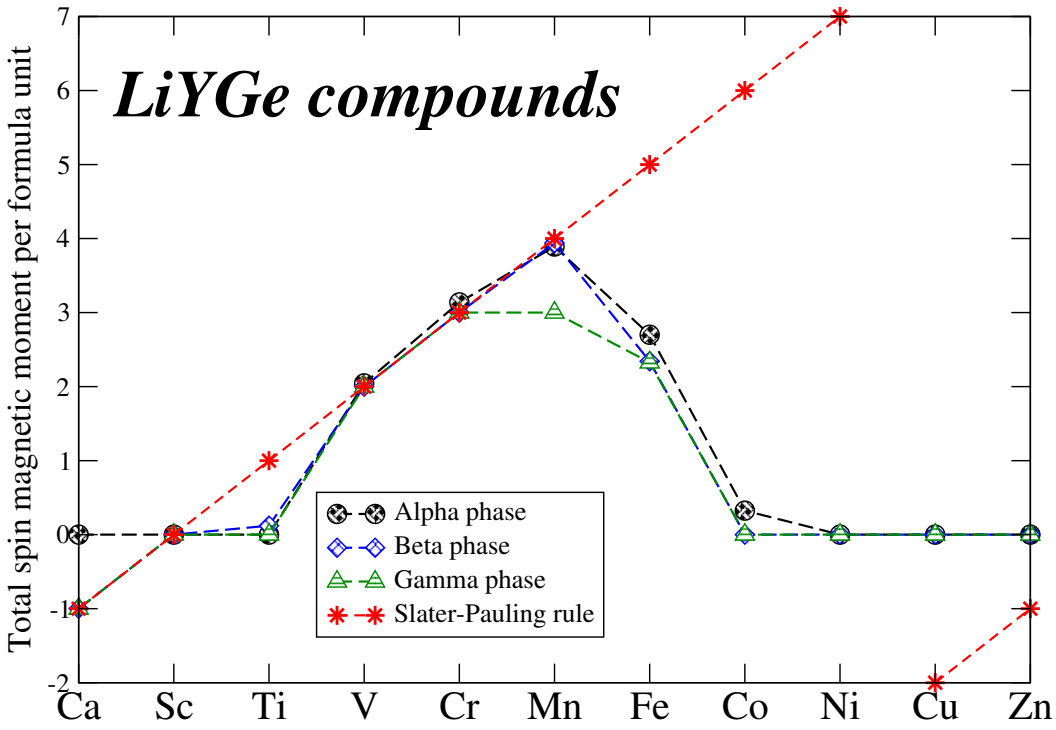


Figure 4. Total spin magnetic per formula unit in μ_B units as a function of the Y chemical element. The red lines represent the ideal Slater–Pauling rules for half-metallicity: $M_t = Z_t$-8 for Y = Ca to Ni, and $M_t = Z_t$-18 for Y = Cu or Zn.

4. Summary and Conclusions

Half-metallic semi-Heusler compounds are at the forefront of current scientific research due to their potential use in spintronic devices. Unlike other semi-Heuslers, $p^0(d^0)$-d compounds can crystallize in three different variations of the $C1_b$ lattice structure, known as the α, β, and γ phases, where the sequence of the atoms in the unit cell changes. Using state-of-the-art ab initio electronic band-structure calculations, we focus on the LiYGa and LiYGe p^0-d Heusler compounds, where Y ranges from Ca to Zn. We examine the structural, electronic, and magnetic properties of these compounds in relation to the three possible variants of the $C1_b$ structure. Our results suggest that all compounds prefer to crystallize in the β and γ phases. For both the β and γ phases, each compound has similar properties dictated by the fact that the Y and Ga/Ge atoms are nearest neighbors. Among the studied compounds, the ones being half-metallic magnets follow a Slater–Pauling behavior with respect to their total spin magnetic moment, which can be explained by a band-structure analysis. Notably, LiVGa, LiVGe, LiMnGa, and LiCrGe are (almost) half-metallic ferromagnets across all three phases and thus are of particular interest for applications.

We expect our results to pave the way for further experimental and theoretical studies of these compounds, which are likely to find several applications in spintronics and magnetoelectronics.

Author Contributions: Both authors (K.Ö. and I.G.) have equally contributed to all stages of the present study and manuscript preparation. All authors have read and agreed to the published version of the manuscript.

Funding: This research received no external funding

Data Availability Statement: The data presented in this study are available on request from the corresponding author.

Conflicts of Interest: The authors declare no conflicts of interest.

Abbreviations

The following abbreviations are used in this manuscript:

DOS	Density of States
f.u.	formula unit
FPLO	Full-potential nonorthogonal local-orbital minimum-basis band-structure approach
GGA	Generalized gradient approximation
PBE	Perdew–Burke–Ernzerhof

References

1. Heusler, F. Über magnetische manganlegierungen. *Verh. Dtsch. Phys. Ges.* **1903**, *12*, 219.
2. Heusler, F.; Take, E. The nature of the Heusler alloys. *Phys. Z.* **1912**, *13*, 897. [CrossRef]
3. Webster, P.J.; Ziebeck., K.R.A. Alloys and Compounds of *d*-Elements with Main Group Elements. Part 2. In *Landolt-Börnstein, New Series, Group III, Vol 19c*; Wijn, H.R.J., Ed.; Springer: Berlin/Heidelberg, Germany, 1988; pp. 75–184.
4. Ziebeck, K.R.A.; Neumann, K.-U. Magnetic Properties of Metals. In *Landolt-Börnstein, New Series, Group III, Vol 32/c*; Wijn, H.R.J., Ed.; Springer: Berlin/Heidelberg, Germany, 2001; pp. 64–414.
5. Kawasaki, J.K.; Chatterjee, S.; Canfield, P.C. Full and half-Heusler compounds. *MRS Bull.* **2022**, *47*, 555. [CrossRef]
6. Graf, T.; Felser, C.; Parkin, S.S.P. Simple rules for the understanding of Heusler compounds. *Prog. Solid State Chem.* **2011**, *39*, 1. [CrossRef]
7. Bachagha, T; Sunol, J.-J. All-*d*-Metal Heusler Alloys: A Review. *Metals* **2023**, *13*, 111. [CrossRef]
8. De Paula, V. G.; Reis, M. S. All-*d*-Metal Full Heusler Alloys: A Novel Class of Functional Materials. *Chem. Mater.* **2021**, *33*, 5483. [CrossRef]
9. Fortunato, N. M.; Li, X.; Schönecker, S.; Xie, R.; Aubel, A.; Scheibel, F.; Opahle, I.; Gutfleisch, O.; Zhang, H. High-Throughput Screening of All-d-Metal Heusler Alloys for Magnetocaloric Applications. *Chem. Mater.* **2024**, *36*, 6765. [CrossRef]
10. Galanakis, I; Dederichs, P.H.; Papanikolaou, N. Origin and Properties of the Gap in the Half-Ferromagnetic Heusler Alloys. *Phys. Rev. B* **2002**, *66*, 134428. [CrossRef]
11. Galanakis, I; Dederichs, P.H.; Papanikolaou, N. Slater-Pauling Behavior and Origin of the Half-Metallicity of the Full-Heusler Alloys. *Phys. Rev. B* **2002**, *66*, 174429. [CrossRef]
12. Katsnelson, M.I.; Irkhin, V.Y.; Chioncel, L.; Lichtenstein, A.I.; de Groot, R.A. Half-metallic ferromagnets: From band structure to many-body effects. *Rev. Mod. Phys.* **2008**, *80*, 315. [CrossRef]
13. Hirohata, A.; Takanashi, K. Perspectives of Heusler compounds. *J. Phys. D Appl. Phys.* **2014**, *47*, 193001. [CrossRef]
14. Spintronics. *From Materials to Devices*; Felser, C., Fecher, G.H., Eds.; Springer: Berlin/Heidelberg, Germany, 2013.
15. Fong, C.Y.; Pask, J.E.; Yang, L.H. (Eds.) Half-Metallic Materials and Their Properties. In *Series on Materials for Engineering*; Imperial College Press: London, UK, 2013; Volume 2.
16. Alloys, H. Properties, Growth, Applications. In *Springer Series in Materials Science*; Felser, C., Hirohata, A., Eds.; Springer International Publishing: Berlin/Heidelberg, Germany, 2018; Volume 222.
17. Galanakis,I.; Özdoğan, K.; Şaşıoğlu, E. Spin-filter and spin-gapless semiconductors: The case of Heusler compounds. *AIP Adv.* **2016**, *6*, 055606. [CrossRef]
18. Gillessen, M.; Dronskowski, R. A combinatorial study of full Heusler alloys by first-principles computational methods. *J. Comput. Chem.* **2009**, *30*, 1290. [CrossRef] [PubMed]
19. Gillessen, M.; Dronskowski, R. A combinatorial study of inverse Heusler alloys by first-principles computational methods. *J. Comput. Chem.* **2010**, *31*, 612. [CrossRef]
20. Ma, J.; Hegde, V.I.; Munira, K.; Xie, Y.; Keshavarz, S.; Mildebrath, D.T.; Wolverton, C.; Ghosh, A.W.; Butler, W.H. Computational investigation of half-Heusler compounds for spintronics applications. *Phys. Rev. B* **2017**, *95*, 024411. [CrossRef]
21. Sanvito, S.; Oses, C.; Xue, J.; Tiwari, A.; Zic, M.; Archer, T.; Tozman, P.; Venkatesan, M.; Coey, M.; Curtarolo, S. Accelerated discovery of new magnets in the Heusler alloy family. *Sci. Adv.* **2017**, *3*, e1602241. [CrossRef] [PubMed]
22. Faleev, S.V.; Ferrante, Y.; Jeong, J.; Samant, M.G.; Jones, B.; Parkin, S.S.P. Unified explanation of chemical ordering, the Slater-Pauling rule, and half-metallicity in full Heusler compounds. *Phys. Rev. B* **2017**, *95*, 045140. [CrossRef]
23. Faleev, S.V.; Ferrante, Y.; Jeong, J.; Samant, M.G.; Jones, B.; Parkin, S.S.P. Heusler compounds with perpendicular magnetic anisotropy and large tunneling magnetoresistance. *Phys. Rev. Mater.* **2017**, *1*, 024402. [CrossRef]
24. He, J.; Rabe, K.M; Wolverton, C. Computationally accelerated discovery of functional and structural Heusler materials. *MRS Bull.* **2022**, *47*, 559. [CrossRef]
25. Galanakis, I.; Özdoğan, K.; Şaşıoğlu, E. High-T_C fully compensated ferrimagnetic semiconductors as spin-filter materials: The case of CrVXAl (X = Ti, Zr, Hf) Heusler compounds. *J. Phys. Condens. Matter* **2014**, *26*, 086003. [CrossRef]
26. Venkateswara, Y.; Gupta, S.; Samatham, S.S.; Varma, M.R.; Enamullah; Suresh, K.G.; Alam, A. Competing magnetic and spin-gapless semiconducting behavior in fully compensated ferrimagnetic CrVTiAl: Theory and experiment. *Phys. Rev. B* **2018**, *97*, 054407. [CrossRef]
27. Damewood, L.; Busemeyer, B.; Shaughnessy, M.; Fong, C.Y, ; Yang, L.H.; Felser, C. Stabilizing and increasing the magnetic moment of half-metals: The role of Li in half-Heusler LiMnZ (Z=N,P,Si). *Phys. Rev. B* **2015**, *91*, 064409. [CrossRef]

28. Dehghan, A.; Davatolhagh, S. d^0-d half-Heusler alloys: A potential class of advanced spintronic materials. *J. Alloys Compd.* **2019**, *773*, 132. [CrossRef]
29. Dehghan, A.; Davatolhagh, S. First principles study of d^0-d half-Heusler alloys containing group-IV, -V, and -VI sp atoms as prospective half-metals for real spintronic applications. *Mat. Chem. Phys.* **2021**, *273*, 125064. [CrossRef]
30. Galanakis, I. Slater–Pauling Behavior in Half-Metallic Heusler Compounds. *Nanomaterials* **2023**, *13*, 2010. [CrossRef] [PubMed]
31. Javari, A. R.; Davatolhagh, S; Dehghan, A. Half-metallic p^0-d half-Heusler alloys with stable structure in ferromagnetic state. *J. Phys. Chem. Solids* **2022**, *166*, 110702. [CrossRef]
32. Aull, T.; Şaşıoğlu, E.; Maznichenko, I.; Ostanin, S.; Ernst, A.; Mertig, I.; Galanakis, I. Abinitio design of quaternary Heusler compounds for reconfigurable magnetic tunnel diodes and transistors. *Phys. Rev. Materials* **2019**, *3*, 124415. [CrossRef]
33. Koepernik, K.; Eschrig, H. Full-potential nonorthogonal local-orbital minimum-basis band-structure scheme. *Phys. Rev. B* **1999**, *59*, 1743. [CrossRef]
34. Kopernik, K. Full Potential Local Orbital Minimum Basis Bandstructure Scheme User's Manual. Available online: https://journals.aps.org/prb/abstract/10.1103/PhysRevB.59.1743 (accessed on 1 June 2024).
35. Perdew, J.P.; Burke, K.; Ernzerhof, M. Generalized Gradient Approximation Made Simple. *Phys. Rev. Lett.* **1996**, *77*, 3865. [CrossRef]
36. Monkhorst, H.J.; Pack, J.D. Special points for Brillouin-zone integrations. *Phys. Rev. B* **1976**, *13*, 5188. [CrossRef]

Disclaimer/Publisher's Note: The statements, opinions and data contained in all publications are solely those of the individual author(s) and contributor(s) and not of MDPI and/or the editor(s). MDPI and/or the editor(s) disclaim responsibility for any injury to people or property resulting from any ideas, methods, instructions or products referred to in the content.